



Corrosion and cell viability studies of graphite-like hydrogenated amorphous carbon films deposited on bare and nitrided titanium alloy



Adélia Moreira Marques dos Santos^a, Ronaldo Junio Campos Batista^a, Leo Anderson Meira Martins^b, Mariana Ilha^b, Moema Queiroz Vieira^b, Douglas Rodrigues Miquita^c, Fátima Costa Rodrigues Guma^b, Iduvirges Lourdes Müller^d, Taíse Matte Manhabosco^{a,*}

^a Departamento de Física, Universidade Federal de Ouro Preto, Campus Universitário Morro do Cruzeiro/ICEB/DEFIS/35400-000, Ouro Preto, Minas Gerais, Brazil

^b Departamento de Bioquímica, ICBS, Universidade Federal do Rio Grande do Sul, rua Ramiro Barcelos 2600-Anexo I, CEP 90035-003 Porto Alegre, Rio Grande do Sul, Brazil

^c Centro de Microscopia da Universidade Federal de Minas Gerais, Universidade Federal de Minas Gerais, CEP 31270-901 Belo Horizonte, Brazil

^d Departamento de Metalurgia, Laboratório de Pesquisa em Corrosão, Universidade Federal do Rio Grande do Sul, Av. Bento Gonçalves 9500/75/232, 91501-970 Porto Alegre, Rio Grande do Sul, Brazil

ARTICLE INFO

Article history:

Received 5 November 2013

Accepted 23 January 2014

Available online 1 February 2014

Keywords:

A. Graphite-like a-C:H films

B. EIS

C. Corrosion resistance

B. AFM

ABSTRACT

This work presents a study of corrosion resistance and cell viability of carbon films on bare and nitrided Ti–6Al–4V. Films deposited on bare alloy significantly improve the corrosion resistance. Unexpectedly, films deposited on nitrided alloy present delamination and cracking after 16 days. We associate film failure with the presence of pores combined with a weak film/substrate interaction that allows diffusion of ions at the interface. We found that films tend to diminish the osteoblastic cell viability and the observed variations on film roughness do not improve cell viability.

© 2014 Elsevier Ltd. All rights reserved.

1. Introduction

Ti–6Al–4V alloy has become one of the most popular biomaterials in the last four decades due to its good properties such as high corrosion resistance, low density, biocompatibility (conferred by the thin and compact oxide (TiO₂) spontaneously formed on its surface in the presence of oxygen) and elasticity modulus (110 GPa), which is about half of that of stainless steel [1–3]. However, in some applications like hip and knee joints better wear resistance is required, which is not conferred by the alloy [4]. Wear resistance and also surface hardness can be increased by surface thermochemical treatments such as plasma nitriding, plasma ion nitriding and laser gas assisted nitriding [5–8]. It has also been shown that the nitriding process can improve the corrosion and tribocorrosion resistance depending on the nitriding conditions [9,10]. Other surface engineering methods that may be used to improve hardness, wear and/or corrosion resistance of titanium and its alloys are overlay coatings like nitride coatings, boride coatings and hard amorphous carbon coatings [11–16].

The overlay coatings named diamond-like carbon (DLC) are a relatively new class of amorphous carbon coatings that have been

studied for biomedical applications due to their hardness, wear resistance, corrosion resistance, bio and hemocompatibilities. In addition, such chemically inert coatings act as a protective barrier that hinders ion release from the titanium alloy or other substrates preventing health problems like toxicity, allergic response and carcinogenic reactions depending on the ion [17]. Thus, ion release and corrosion resistance of the coatings are crucial features to be considered when an implant is placed in a living body. There may be strong foreign body reactions such as implant failure, thrombosis and fibrous capsule formation, infections and also the aforementioned carcinogenic reactions if the coating degrades [18,19]. In particular, it is worth mentioning the work of Gutensohn et al. [18] who studied the biocompatibility and metal ions release of DLC coated 316 L stainless steel stents. The authors demonstrated that DLC coatings significantly reduced the metal ions release (nickel, chromium, manganese and molybdenum) from the stents and, as a consequence, platelet activation was diminished. It is important to point out that platelet activation is an important trigger of thrombosis and, therefore, should be avoided.

The combination of two surface engineering methods has also been applied aiming to further improve the biomaterial properties [9,20]. For instance, Avelar-Batista et al. [20] have successfully increased the wear resistance of Ti–6Al–4V by combining a nitriding pre-treatment with a DLC coating. The authors found that the

* Corresponding author. Tel.: +55 31 3559 1675.

E-mail address: taise@iceb.ufop.br (T.M. Manhabosco).

nitriding process increases the load support for the hard DLC coating. It provides a gradual change in the surface hardness that reduces the degree of plastic deformation of the underlying material. In this contribution a study is presented on cell viability and corrosion behavior of Ti–6Al–4V modified by two different methods: graphite-like hydrogenated amorphous carbons (GLCH) overlay coating and nitriding process plus GLCH overlay coating.

2. Experimental

Samples with a 38 mm diameter and mean thickness of 17 mm were obtained from a Ti–6Al–4V (grade 5) bar. Samples were ground with SiC emery paper to 800 grit and polished with colloidal silica. After polishing the samples were ultrasonically cleaned in acetone for 10 min followed by rinsing in methanol and deionized water.

Some samples were nitrided in a gas mixture of 10% Ar, 50% H₂ and 40% N₂ at 300 Pa for 10 h. The process temperature (1073 K) was chosen below the transition temperature of the alloy (1228 K). The presence of a 1 µm thick nitrided layer was observed as previously characterized [10].

Films were deposited both on the polished and on the nitrided samples using a Radio Frequency (13.56 MHz) Plasma Assisted Chemical Vapor Deposition (RF PACVD) technique. Prior to deposition, samples were cleaned by sputtering with Ar during 20 min. The deposition was performed at 1.5 Pa with acetylene (CH₃)₂ flowing at a rate of 50 sccm (standard cubic centimeters per minute) for 2 h. The negative self-bias voltage of the RF powered electrodes was 1000 V. Films with about 4 µm thickness were obtained in the deposition process. The coatings were analyzed by Raman spectroscopy performed with a NTEGRA Spectra Nanofinder (NT-MDT) operating at 514.5 nm excitation at room temperature.

The corrosion behavior of the films deposited on bare and on nitrided alloy was evaluated by potentiodynamic polarization curves and electrochemical impedance spectroscopy (EIS) measurements. Impedance data for 1 h, 48 h, 7 days, 16 days, 23 days, 30 days and 37 days of immersion were acquired by a potentiostat (AUTOLAB PGSTAT 30) and a frequency response analyzer (FRA) system operating at open circuit potential (OCP) in a frequency range from 100 kHz to 3 MHz with a sinusoidal perturbation of 10 mV (Rms). All tests were carried out in a three-electrode cell containing phosphate buffer saline (PBS) solution in order to simulate the human body environment. The solution (pH = 7.1) is composed by 8 g L⁻¹ NaCl; 0.2 g L⁻¹ KCl; 0.594 g L⁻¹ Na₂HPO₄ and 0.2 g L⁻¹ KH₂PO₄. A saturated calomel reference electrode was used as reference electrode and a platinum (Pt) wire as counter electrode.

To evaluate cell viability on the films, 4 × 10⁴ of murine femur osteoblastic cells (F-OST) obtained from the Cell Bank of Rio de Janeiro (HUCFF, UFRJ, RJ) were seeded on titanium pieces placed on 12 well culture plates (Nunc, Roskilde, Denmark) for 24 h. Cells seeded on the plastic bottom (without titanium scaffolds) were considered the experiment control since they represent the normal culture condition. The cells were maintained in Dulbecco's Modified Eagle's Medium (DMEM, Invitrogen, Carlsbad, CA, USA) supplemented with 15% foetal bovine serum (FBS, Cultilab, Campinas, Brazil) and 2 g/L HEPES buffer (pH 7.4) in a humidified atmosphere with 5% CO₂ at 37 °C. The colorimetric MTT assay was used to evaluate cell viability by quantifying the cellular dehydrogenase activities that reduce MTT (3-(4,5-dimethylthiazolyl)-2,5-diphenyl-2H-tetrazolium bromide) to a purple formazan salt. After 48 h of culture, the cells were incubated with 1 mg/mL MTT for 2 h at 37 °C in the dark. The cells were then lysed in dimethylsulfoxide (DMSO, Sigma Inc., Saint Louis, USA), the purple formazan crystals were dissolved, and the lysates were measured in a microplate spectrophotometer (Spectra Max 190, Molecular Devices, USA) at

570 nm and 630 nm. Proteins were quantified by Lowry's modified assay [21]. Results were expressed as MTT absorbance per µg of protein. The data were expressed as the means ± SE of the mean. One-way ANOVA was used to analyze the effect of the treatment time. When indicated, a *post hoc* Duncan multiple range test was performed. The results were considered statistically different when the *p* values were equal to or less than 0.05.

3. Results and discussion

3.1. Film characterization

Films deposited on Ti–6Al–4V and on nitrided Ti–6Al–4V were morphologically characterized by AFM (Fig. 1). Films deposited on bare Ti–6Al–4V present low Rms roughness (8.9 nm) and are composed of small compact grains with the average size of 0.2 µm. Films deposited on nitrided samples are composed of agglomerates of small grains with non-homogeneous size and higher Rms roughness (70.4 nm). Such agglomerates are larger than the small compact grains of films deposited on bare alloy. The observed increase (about six times) of surface roughness of the nitride alloy compared to the bare one is due to the sputtering in the nitriding process. The surface roughness affects the coating morphology, which can also be affected by the substrate chemical composition and by secondary electron emission from the substrates. The secondary electron emission from different substrates increases the plasma intensity differently, which may result in different coating properties and morphology [22].

As previously reported [23], the Raman spectra of our films presents the characteristic D and G peaks, the D peak lying at approximately 1385 cm⁻¹ and the G peak lying at around 1569 cm⁻¹. The term diamond-like carbon (DLC) has been employed to designate several kinds of carbon films. In order to be more specific, we adopt the nomenclature used by Casiraghi et al. [24]. Those authors characterize films with a hydrogen content lower than 20% as being graphite-like hydrogenated amorphous carbons (GLCH). The Raman spectra can be used to calculate the hydrogen content of the carbon films [23]: The hydrogen content of the films investigated in this study is about 16%.

3.2. Polarization curves

Fig. 2(A and B) shows polarization curves for GLCH films deposited on Ti–6Al–4V and nitrided Ti–6Al–4V, respectively. It can be seen that the GLCH films present similar behavior both deposited on bare and nitrided Ti–6Al–4V. Films present low current densities indicating a superior corrosion protection conferred on the substrates.

The protective efficiency and coating porosity were determined from the polarization curves by empirical equations [25,26].

$$P_i = 100 \left(1 - \frac{i_{corr}}{i_{corr}^0} \right) \quad (1)$$

$$F = \left(\frac{R_p(\text{substrate})}{R_p(\text{coating-substrate})} \right) 10^{\frac{|\Delta E_{corr}|}{\beta_a}} \quad (2)$$

where P_i is the protective efficiency, i_{corr} and i_{corr}^0 are the corrosion current densities in the presence and absence of the coating, F is the coating porosity, R_p the polarization resistance of the substrate or of the coated substrate, ΔE_{corr} is the potential difference between the free corrosion potentials of the coated alloy and the bare substrate and β_a , the anodic Tafel slope for the substrate.

The protective efficiency and coating porosity of the films deposited on Ti–6Al–4V were about 97% and 0.01%, while those

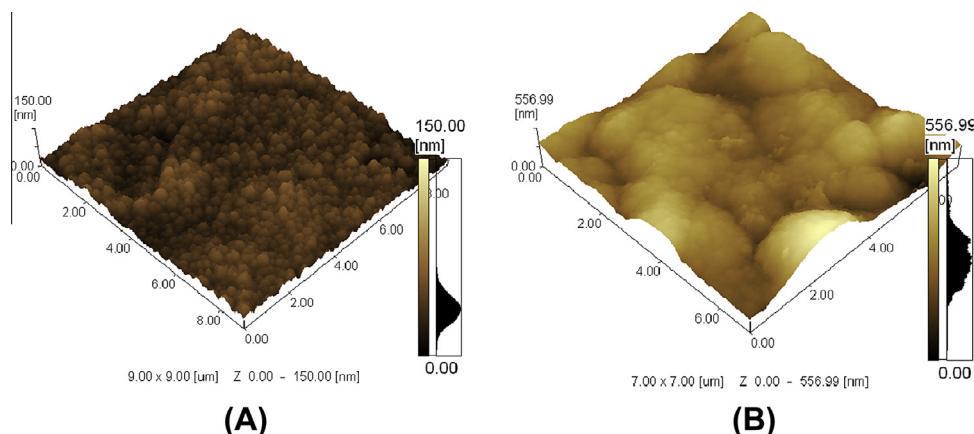


Fig. 1. Atomic force microscopy images for films deposited on (A) bare Ti-6Al-4V and (B) nitrided Ti-6Al-4V.

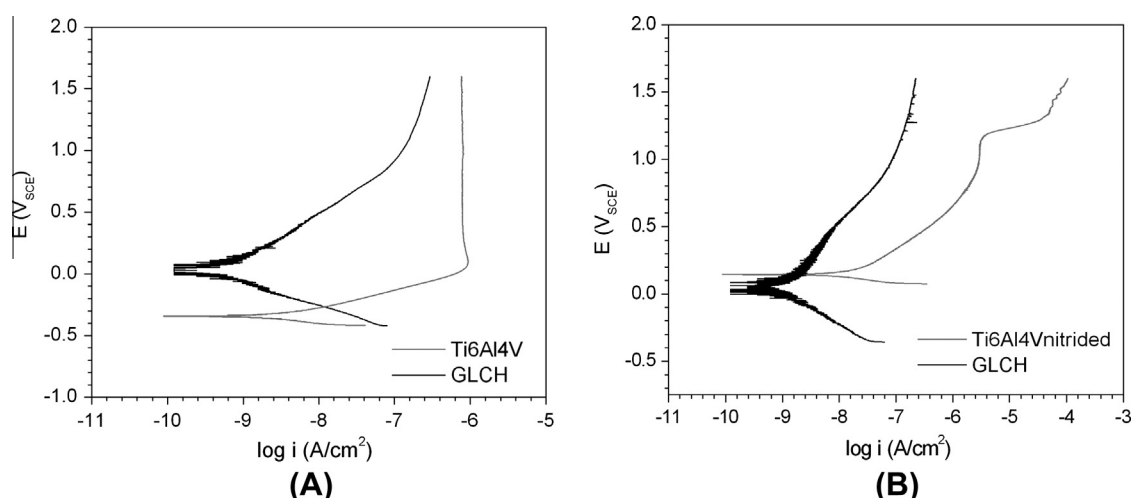


Fig. 2. Potentiodynamic polarization curves for GLCH films deposited on bare (A) and nitrided Ti-6Al-4V (B). The curves of the substrates are also shown. Experiments were performed in PBS solution at a sweep rate of 0.167 mV/s.

values for films deposited on nitrided sample were about 95% and 0.02%.

It is well known that the titanium and its alloys present a passive behavior in solutions that simulate the body environment due to the formation of a protective oxide layer [27]. With this alloy (Ti-6Al-4V) it is possible to observe low anodic current densities ($0.8 \mu\text{A}/\text{cm}^2$) in a wide range of potentials (from 0 to $1.6 V_{\text{SCE}}$). Comparing the bare alloy to nitrided alloy, it is possible to observe an increase in the corrosion potential associated with the formation of a nitrided layer. Low anodic current densities (about $1.5 \mu\text{A}/\text{cm}^2$) are observed until $1.1 V_{\text{SCE}}$. Afterwards an anodic peak is observed that may correspond to the oxidation of TiN to TiO_2 , according to Heide and Schultze [28]. Some breaks observed in the curve of GLCH deposited on nitrided Ti-6Al-4V at high overpotentials (above $1.1 V_{\text{SCE}}$) could be related to the oxidation of the substrate (TiN to TiO_2).

3.3. EIS

Fig. 3 shows Bode plots of the EIS data obtained for GLCH deposited on bare Ti-6Al-4V and nitrided Ti-6Al-4V after 1 h of sample exposure to the simulated body environment. The similar behavior of both curves reveals that the electrochemical behavior of samples (GLCH covered alloy and GLCH covered nitrided alloy) is primarily determined by the GLCH coating. The phase angle in that figure

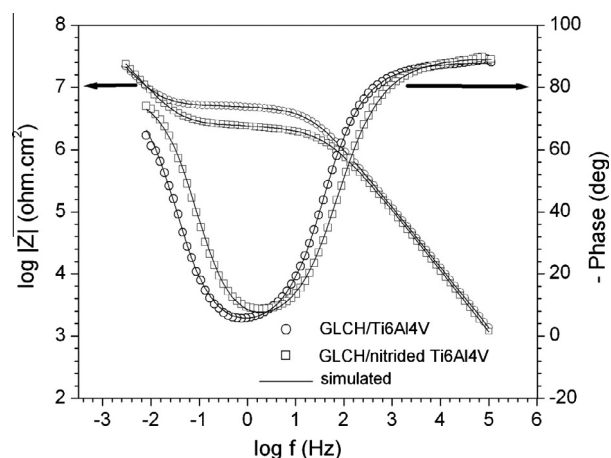


Fig. 3. Bode plots of GLCH films deposited on bare and nitrided Ti-6Al-4V immersed in PBS solution for a 1 h period. The solid lines show fit of the data by the equivalent circuits shown in Fig. 3.

shows two mainly capacitive regions: one at high frequencies (about 10^4 Hz) and another at low frequencies (below 10^{-4} Hz). Those regions are of particular interest because they give information about GLCH film (high-frequency region) and information

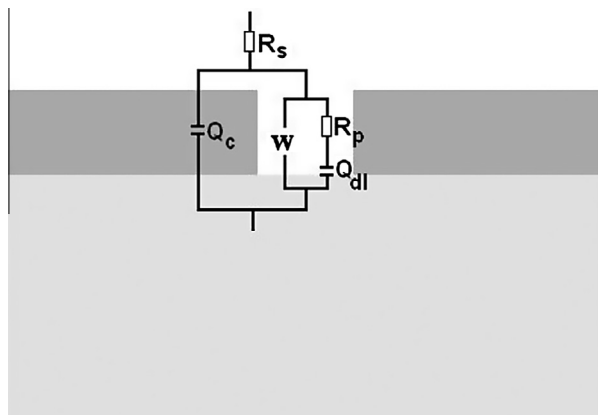


Fig. 4. Schematic diagram of equivalent circuit for GLCH films deposited on bare Ti–6Al–4V. The same equivalent circuit is also employed to simulate films deposited on nitrided Ti–6Al–4V for immersion times inferior to 16 days. For immersion times greater than 16 days the electrochemical behavior of films deposited on nitrided Ti–6Al–4V is well described by the circuit shown in Fig. 7.

about the processes related to reactions at the electrolyte/substrate interface taking place in the pores of GLCH films (low-frequency region).

In order to understand the EIS measurements shown in Fig. 3, we fit the impedance data using an equivalent electrical circuit, shown in Fig. 4, that is representative of the physical processes taking place in the system under investigation. The circuit is composed of an electrolyte solution resistance (R_s); a pore resistance (R_p); a Warburg element (W) that represents the diffusion of ions from the solution to the small pores and from the corroding substrate to the solution; two constant phase elements (CPE), represent non-ideal capacitors, one regarding the GLCH film (Q_c) and another regarding the (Q_{dl}) double-layer capacitance at the electrolyte/substrate interface.

In the frequency range studied the GLCH film resistance is much higher than the impedance of the other proposed circuit elements.

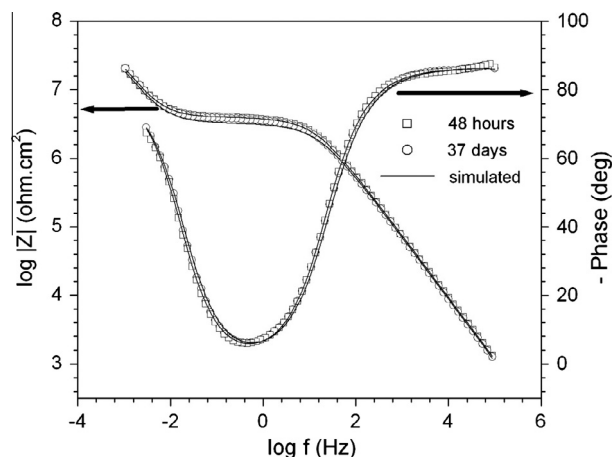


Fig. 5. Bode plots of GLCH films deposited on bare Ti–6Al–4V immersed in PBS solution for 48 h and 37 days. The solid lines show fit of the data by the equivalent circuits shown in Fig. 3.

In that case we consider it infinite, or an open circuit, and represent the GLCH film by a constant phase element only (Q_c). For the same reason there is no resistance parallel to the Q_{dl} element, the small porous area combined with the good corrosion resistance of the Ti–6Al–4V alloy makes the resistance to polarization at the electrolyte/substrate interface also too high in comparison to the impedance of the remaining circuit elements. Thus, the proposed circuit is able to fit the data reproducing the predominance of capacitive behaviors at high (Q_c) and low (Q_{dl}) frequencies observed in Fig. 3. In Tables 1 and 2, which show circuit element values for films deposited on bare and nitrided alloy respectively, it is possible to see that the values of the capacitance of GLCH films (Q_c) are in the range between 1.3 nF cm^{-2} and 2.0 nF cm^{-2} . Such capacitance values are similar to those found by other authors for hydrogenated amorphous carbon films [29,30], which corroborates our circuit model. The double-layer capacitance at the electrolyte/sub-

Table 1

Fitting parameters of the impedance spectrum performed along the immersion times for GLCH deposited on bare Ti–6Al–4V.

	1 h	48 h	7 days	16 days	23 days	30 days	37 days
R_s ($\Omega \text{ cm}^2$)	20	20	20	19	19	20	19
Q_c (nF cm^{-2})	1.8	2.0	2.0	2.0	2.0	2.1	2.1
n_c	0.97	0.96	0.97	0.97	0.97	0.97	0.96
Y_0 ($\text{nS s}^{1/2}$)	6.5	6.7	8.2	7.9	7.9	8.9	8.8
Q_{dl} ($\mu\text{F cm}^{-2}$)	1.8	1.9	1.9	1.9	1.8	1.9	1.9
n_{dl}	0.89	0.9	0.91	0.90	0.90	0.91	0.89
R_p ($\text{k}\Omega \text{ cm}^2$)	5190	4000	3510	3820	3930	3450	3380

Table 2

Fitting parameters of the impedance spectrum performed along the immersion times for GLCH deposited on nitrided Ti–6Al–4V.

	1 h	48 h	7 days	16 days	23 days	30 days	37 days
R_s ($\Omega \text{ cm}^2$)	20	20	20	18	18	18	18
Q_c (nF cm^{-2})	1.4	1.6	1.3	1.4	1.4	1.4	1.4
n_c	1	0.99	1	1	1	1	1
Y_0 ($\text{nS s}^{1/2}$)	15	21	42	27	26	29	28
Q_{dl1} ($\mu\text{F cm}^{-2}$)	1.4	1.5	1.5	1.5	1.4	1.5	1.5
n_{dl1}	0.90	0.90	0.92	0.90	0.90	0.90	0.89
R_p ($\text{k}\Omega \text{ cm}^2$)	2570	2190	2070	2170	2160	1900	1990
R_{ck} ($\text{k}\Omega \text{ cm}^2$)	–	–	–	910	690	910	710
Q_{dl2} (nF cm^{-2})	–	–	–	3.7	5.0	5.1	5.5
n_{dl2}	–	–	–	0.86	0.84	0.84	0.84

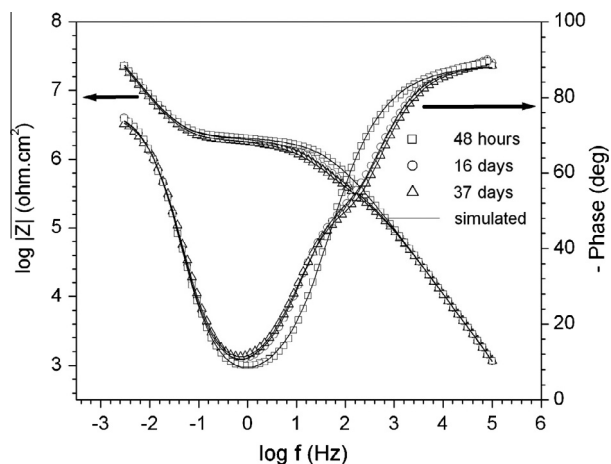


Fig. 6. Bode plots of GLCH films deposited on nitrided Ti-6Al-4V immersed in PBS solution for 48 h, 16 days and 37 days. The solid lines show fit of the data by the equivalent circuits shown in Fig. 3 (48 h) and Fig. 7.

strate interface (Q_{dl}) for bare and nitrided substrate are in the order of $1\text{--}2\ \mu\text{F cm}^{-2}$. The range of $\mu\text{F cm}^{-2}$ is a well-known value for a metallic and nitrided surface immersed in an electrolytic solution with low resistance (as observed in Tables 1 and 2) [31,32].

According to Tables 1 and 2, the pore resistance (R_p) of films deposited on bare alloy is almost twice as large as the resistance of films deposited on nitrided alloy. Considering that the pore resistance is well described by:

$$R = \rho \frac{L}{A} \quad (3)$$

where ρ is the solution resistance, L is the pore length and A is the pore area, it is reasonable to suppose that the pore area of films deposited on nitrided alloy is bigger than that of films deposited on bare alloy. In addition, the lower values of the Warburg coefficient (which is inversely proportional to the magnitude of admittance (Y_0)) shown in Tables 1 and 2 of films deposited on nitrided alloy in comparison to that of films deposited on bare alloy indicates that the pore area in films deposited on nitrided alloy is bigger than that of pores in films deposited on bare alloy. The Warburg coefficient (σ_w) is related to the area according to the following expression [33]:

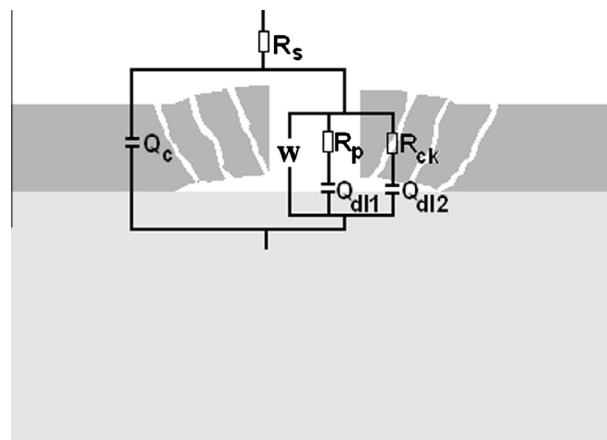


Fig. 8. Schematic diagram of equivalent circuit for GLCH films deposited on nitrided alloy after 16 days of immersion in PBS solution.

$$\sigma_w = \frac{RT}{n^2 F^2 A \sqrt{2}} \left(\frac{1}{C_0 \sqrt{D_0}} + \frac{1}{C_R \sqrt{D_R}} \right) \quad (4)$$

where R is the gas constant; T the temperature; n the number of electrons involved; F the Faraday constant; A the surface area of the electrode; C_0 the concentration of the oxidant; D_0 the diffusion coefficient of the oxidant; C_R the concentration of the reductant; and D_R is the diffusion coefficient of the reductant.

The indicative that the pores in films deposited on nitrided alloy are larger than those of films deposited on bare alloy is also observed in the lower protective efficiency and higher coating porosity obtained from polarization curves.

The admittance values (Y_0) of both systems slowly increase over time due to the corrosion process that injects ions from the substrate into the electrolyte. Such a process also decreases pore resistance.

In spite of the presence of pores, the electrochemical behavior of films deposited on bare alloy does not change during the time tested as can be seen in Fig. 5, which shows the bode plot for 48 h and 37 days. This result indicates that films deposited on bare alloy present excellent corrosion resistance. On the other hand, films deposited on nitrided alloy change their electrochemical

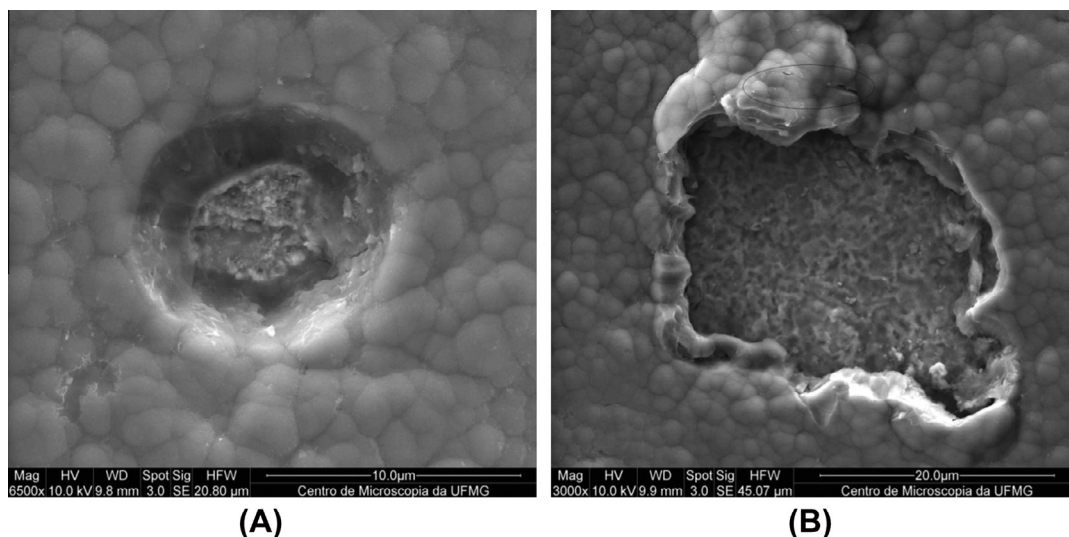


Fig. 7. SEM image of a characteristic pore (A) on GLCH film deposited on nitrided alloy and a delaminated region (B) after 37 days of immersion in PBS solution.

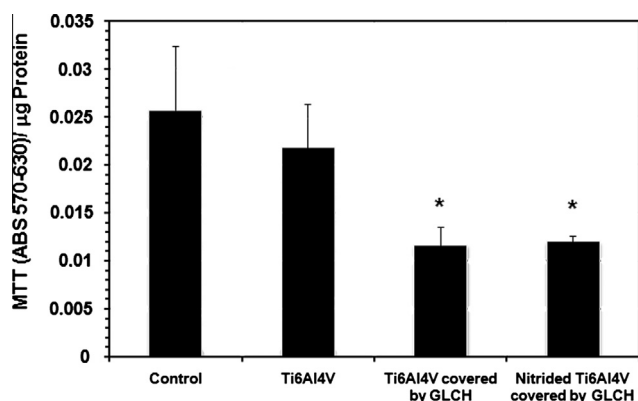


Fig. 9. The F-OST cell viability through MTT. *Indicates significant differences between groups ($p \leq 0.05$). Data was expressed as mean \pm SEM ($n = 3$).

behavior after 16 days as can be seen in Fig. 6, which shows the bode plot of GLCH deposited on nitrided samples for 48 h, 16 and 37 days. In order to understand the observed change in the electrochemical behavior we have looked for morphological changes in the film by means of SEM images. Fig. 7A shows the SEM image of a characteristic pore of the film while Fig. 7B shows an area in which part of the film has been delaminated. At the borders of the defect it is possible to see a crack (circled area) and irregularities due to the cracking of the film. Such an image combined with the presence of pores suggests the following process: (i) water and ions penetrate through the pores reaching the metal/film interface; (ii) loss of adhesion between metal and film occurs due to corrosion and penetration of fluid; (iii) the hard film cracks to release the tension due to fluid penetration at the interface. To further investigate such an hypothesis we include new circuit elements to represent a delaminated and cracked area around the pore as shown in Fig. 8. The new circuit is composed of a solution resistance (R_s); a pore resistance (R_p); a crack resistance (R_{ck}) that represents the electrolytic conduction at the cracked film; a Warburg element (W); three CPE, one for the GLCH film (Q_c), another representing the (Q_{dl1}) double-layer capacitance at substrate/electrolyte interface in the pore and another for the (Q_{dl2}) double-layer capacitance at the substrate/electrolyte interface in the detached and cracked regions of the film. As can be seen in Fig. 6 the new circuit fits very well the electrochemical behavior after 16 days, which supports the proposed process.

The double-layer capacitance (Q_{dl2}) in detached and cracked regions of the film and mainly the crack resistance (R_{ck}) are expected to be oscillating values as observed. This is because new cracks will be formed during the immersion days and the cracked film will be released, so the region is very unstable and changed its configuration throughout the days.

From the results discussed above, a question that naturally arises is why the delamination and cracking occur only in the films deposited on nitrided alloy during the time tested. It should be kept in mind that the nitrided alloy is rougher than the bare alloy, which should promote an anchor or interlocking effect. A possible explanation could be a weaker interaction between the GLCH film and the nitrided substrate compared to the interaction between the GLCH film and the bare substrate. In fact, in a recent work [23] we used AFM force curve measurements to show that the interactions between a diamond covered tip and a nitrided surface are much less intense than those between the same tip and a bare surface, which suggests that the interaction between hard carbon films and the nitrided alloy is weaker than the interaction between hard carbon films and the bare alloy.

3.4. Cell culture

The MTT assay evaluated the F-OST cell viability by measuring cellular dehydrogenase activities of living cells whose results are presented in Fig. 9. The cell viability on Ti-6Al-4V pieces was similar to that found in control cells, which was better when compared to the other groups. Considering the similarity regarding the results found in Ti-6Al-4V covered by GLCH and nitrided Ti-6Al-4V covered by GLCH, it can be suggested that the GLCH cover could present some interference on F-OST cell viability. Although the GLCH deposited on nitrided samples is rougher than that deposited on bare Ti-6Al-4V, the level of roughness did not influence cell viability.

4. Conclusion

GLCH films deposited on bare Ti-6Al-4V alloy are homogeneous and composed by small, compact grains while those deposited on the nitrided alloy present a rougher morphology composed by not homogeneously sized grains.

Films deposited on both substrates present high corrosion resistance, however they contain pores that allow a diffusion process and corrosion of the substrate. After 16 days of immersion, films deposited on the nitrided alloy change their electrochemical behavior while films deposited on bare alloy remain unchanged. Our results point out that such a change in the electrochemical behavior is due to substrate/film interface degradation, film delamination and cracking. We associate the higher durability of films deposited on bare alloy compared with films deposited on nitrided alloy with the higher interaction between the film and the bare alloy, which is supported by previous AFM force curve measurements.

The GLCH films diminish the viability of osteoblast cells when compared with the uncovered alloy. The roughness of the tested surface showed no influence on this behavior.

Acknowledgments

The authors wish to acknowledge the financial support of the Brazilian government agencies CNPq, CAPES, FAPEMIG and INCT em Nanomateriais de Carbono (CNPq/MCTI).

References

- [1] M. Niinomi, Mechanical properties of biomedical titanium alloys, *Mater. Sci. Eng. A243* (1998) 231–236.
- [2] S.L. Assis, S. Wolyne, I. Costa, Corrosion characterization of titanium alloys by electrochemical techniques, *Electrochim. Acta* 51 (2006) 1815–1819.
- [3] J.E.G. González, J.C. Mirza-Rosca, Study of the corrosion behavior of titanium and some of its alloys for biomedical and dental implant applications, *J. Electroanal. Chem.* 471 (1999) 109–115.
- [4] M. Niinomi, Mechanical biocompatibilities of titanium alloys for biomedical applications, *J. Mech. Behav. Biomed. Mater.* 1 (2008) 30–42.
- [5] T.M. Muraleedharan, E.I. Meletis, Surface modification of pure titanium and Ti-6Al-4V by intensified plasma ion nitriding, *Thin Solid Films* 221 (1992) 104–113.
- [6] B.S. Yilbas, C. Karatas, Usan, O. Keles, I.Y. Usta, M. Ahsan, CO₂ laser gas assisted nitriding of Ti-6Al-4V alloy, *Appl. Surf. Sci.* 252 (2006) 8557–8564.
- [7] A. Zhecheva, W. Sha, S. Malinov, A. Long, Enhancing the microstructure and properties of titanium alloys through nitriding and other surface engineering methods, *Surf. Coat. Technol.* 200 (2005) 2192–2207.
- [8] I.M. Pohreluk, V.M. Fedirko, O.V. Tkachuk, R.V. Proskurnyak, Corrosion resistance of Ti-6Al-4V alloy with nitride coatings in Ringer's solution, *Corros. Sci.* 66 (2013) 392–398.
- [9] A.C. Fernandes, F. Vaz, E. Ariza, L.A. Rocha, A.R.L. Ribeiro, A.C. Vieira, J.P. Rivière, L. Pichon, Tribocorrosion behaviour of plasma nitrided and plasma nitrided + oxidised Ti6Al4V alloy, *Surf. Coat. Technol.* 200 (2006) 6218–6224.
- [10] T.M. Manhobosco, S.M. Tamborim, C.B. dos Santos, I.L. Müller, Tribological, electrochemical and tribo-electrochemical characterization of bare and

- nitrided Ti6Al4V in simulated body fluid solution, *Corros. Sci.* 53 (2011) 1786–1793.
- [11] L. Ding, K. Nakasa, M. Kato, T. Inoue, Coating of TiB₂ dispersed Ti₅₀Ni₅₀ superelastic alloy layer onto Ti–6Al–4V alloy by spark and resistance sintering, *Surf. Coat. Technol.* 204 (2010) 1738–1748.
 - [12] H.H. Huang, C.H. Hsu, S.J. Pan, J.L. He, C.C. Chen, T.L. Lee, Corrosion and cell adhesion behavior of TiN-coated and ion-nitrided titanium for dental applications, *Appl. Surf. Sci.* 244 (2005) 252–256.
 - [13] D. Turcio-Ortega, S.E. Rodil, S. Muhl, Corrosion behavior of amorphous carbon deposit in 0.89% NaCl by electrochemical impedance spectroscopy, *Diamond Relat. Mater.* 18 (2009) 1360–1368.
 - [14] E. Liu, H.W. Kwek, Electrochemical performance of diamond-like carbon thin films, *Thin Solid Films* 516 (2008) 5201–5205.
 - [15] T.M. Manhobosco, I.L. Muller, Electrodeposition of diamond-like carbon (DLC) films on Ti, *Appl. Surf. Sci.* 255 (2009) 4082–4086.
 - [16] P. Gupta, E.I. Meletis, Tribological behavior of plasma-enhanced CVD a-C: H films. Part II: Multinanolayers, *Tribol. Int.* 37 (2004) 1031–1038.
 - [17] S. Kobayashi, Y. Ohgoe, K. Ozeki, K. Sato, T. Sumiya, K.K. Hirakuri, H. Aoki, Diamond-like carbon coatings on orthodontic archwires, *Diamond Relat. Mater.* 14 (2005) 1094–1097.
 - [18] K. Gutensohn, C. Beythien, J. Bau, T. Fenner, P. Grewe, R. Koester, K. Padmanaban, P. Kuehn, In vitro analyses of diamond-like carbon coated stents: reduction of metal ion release, platelet activation, and thrombogenicity, *Thromb. Res.* 99 (2000) 577–585.
 - [19] D. Bociaga, K. Mitura, Biomedical effect of tissue contact with metallic material used for body piercing modified by DLC coatings, *Diamond Relat. Mater.* 17 (2008) 1410–1415.
 - [20] J.C. Avelar-Batista, E. Spain, G.G. Fuentes, A. Sola, R. Rodriguez, J. Housden, Triode plasma nitriding and PVD coating: a successful pre-treatment combination to improve the wear resistance of DLC coatings on Ti6Al4V alloy, *Surf. Coat. Technol.* 201 (2006) 4335–4340.
 - [21] G.L. Peterson, Review of the folin phenol protein quantitation method of Lowry, Rosebrough, Farr and Randall, *Anal. Biochem.* 100 (1979) 201–220.
 - [22] K.S. Mogensen, N.B. Thomsen, S.S. Eskildsen, C. Mathiasen, J. Böttiger, A parametric study of the microstructural, mechanical and tribological properties of PACVD TiN coatings, *Surf. Coat. Technol.* 99 (1998) 140–146.
 - [23] T.M. Manhobosco, A.P.M. Barboza, R.J.C. Batista, B.R.A. Neves, I.L. Müller, Corrosion, wear and wear–corrosion behavior of graphite-like a-C: H films deposited on bare and nitrided titanium alloy, *Diamond Relat. Mater.* 31 (2013) 58–64.
 - [24] C. Casiraghi, A.C. Ferrari, J. Robertson, Raman spectroscopy of hydrogenated amorphous carbons, *Phys. Rev. B* 72 (2005) 085401.
 - [25] K. Nozawa, K. Aramaki, One- and two-dimensional polymer films of modified alkanethiol monolayers for preventing iron from corrosion, *Corros. Sci.* 41 (1999) 57–73.
 - [26] B. Matthes, E. Broszeit, J. Aromaa, H. Ronkainen, S.-P. Hannula, A. Leyland, A. Matthews, Corrosion performance of some titanium-based hard coatings, *Surf. Coat. Technol.* 49 (1991) 489–495.
 - [27] A.K. Shukla, R. Balasubramaniam, S. Bhargava, Properties of passive film formed on CP titanium, Ti–6Al–4V and Ti–13.4Al–29Nb alloys in simulated human body conditions, *Intermetallics* 13 (2005) 631–637.
 - [28] N. Heide, J.W. Schultze, Corrosion stability of TiN prepared by ion implantation and PVD, *Nucl. Instrum. Methods Phys. Res. B* 80–81 (1993) 467–471.
 - [29] A. Zeng, E. Liu, I.F. Annergren, S.N. Tan, S. Zhang, P. Hing, J. Gao, EIS capacitance diagnosis of nanoporosity effect on the corrosion protection of DLC films, *Diamond Relat. Mater.* 11 (2002) 160–168.
 - [30] H.-G. Kima, S.-H. Ahn, J.-G. Kim, S.J. Park, K.-R. Lee, Corrosion performance of diamond-like carbon (DLC)-coated Ti alloy in the simulated body fluid environment, *Diamond Relat. Mater.* 14 (2005) 35–41.
 - [31] H.-G. Kim, S.-H. Ahn, J.-G. Kim, S.J. Park, K.-R. Lee, Corrosion performance of diamond-like carbon (DLC)-coated Ti alloy in the simulated body fluid environment, *Diamond Relat. Mater.* 14 (2005) 35–41.
 - [32] S. Rossi, L. Fedrizzi, T. Bacci, G. Pradelli, Corrosion behaviour of glow discharge nitrided titanium alloys, *Corros. Sci.* 45 (2003) 511–529.
 - [33] A.J. Bard, L.R. Faulkner, *Electrochemical Methods*, John Wiley & Sons, New York, 1980.